Journal of Quantitative Spectroscopy & Radiative Transfer 313 (2024) 108827

Contents lists available at ScienceDirect

Journal of Quantitative Spectroscopy and Radiative Transfer

journal homepage: www.elsevier.com/locate/jqsrt

Comparison between ACE and CALIPSO observations of Antarctic polar stratospheric clouds

Léo Lavy [a,*], Peter Bernath [a,b], Michael Lecours [b], Dylan English [a], Michael Fromm [c]

[a] Department of Chemistry and Biochemistry, Old Dominion University, Norfolk, VA 23529, USA
[b] Department of Chemistry, University of Waterloo, Waterloo, ON N2L 3G1, Canada
[c] Naval Research Laboratory, Washington, D.C. 20375, USA

ARTICLE INFO

Keywords:
Atmospheric Chemistry Experiment
CALIPSO
Polar stratospheric clouds
Infrared solar absorption spectroscopy
Satellite remote sensing
Lidar

ABSTRACT

The depletion of stratospheric ozone is catalyzed by polar stratospheric clouds (PSCs) that form in the cold polar winter. The space-based lidar onboard CALIPSO (Cloud-Aerosol Lidar and Infrared Pathfinder Satellite Observations) has been the reference instrument for measuring PSCs. Recently, the infrared transmission spectra recorded by the Fourier transform instrument on the ACE (Atmospheric Chemistry Experiment) satellite has provided measurements of PSC composition. We report on coincident observations made by the CALIPSO and the ACE satellites for three late winter periods (2016, 2018 and 2019) and evaluate CALIPSO's determination of PSC composition relative to ACE's findings. We found that CALIPSO and ACE generally agree well for the detection of nitric acid trihydrate (NAT) clouds. However, CALIPSO detects some NAT clouds where ACE detects supercooled ternary solutions of nitric and sulfuric acid (STS). Similarly, CALIPSO only partially detects ice in ACE's ice clouds. Overall, these results seem to show that CALIPSO's NAT classification might be too inclusive. We also found that supercooled nitric acid (SNA) clouds, a new classification, are labelled as STS by CALIPSO.

1. Introduction

The Montreal Protocol on Substances that Deplete the Ozone Layer (1989) [1] is a remarkable example of a successful policy, as it significantly contributed to mitigating the stratospheric ozone depletion [2]. The role of chlorofluorocarbons (CFCs) was established in 1974 by Molina and Rowland [3]: under stratospheric conditions and in the presence of UV light, chlorine atoms released from CFCs lead to ozone depletion. Fortunately, most of the chlorine is stored in reservoir molecules that do not react with ozone [4].

As it turns out, reservoir molecules such as hydrogen chloride (HCl) and chlorine nitrate ($ClONO_2$) can react on particles of Polar Stratospheric Clouds (PSCs) to produce chlorine gas (Cl_2) and lead to ozone depletion in springtime [5]. Ozone depletion resulting from this mechanism was first observed in the Halley Bay, Antarctica [6]. PSCs form during polar winter and require very cold temperatures in the stratosphere. As climate models predict stratospheric cooling, the frequency of these clouds could be affected [7], thus, they hold significant scientific interest.

The accepted basic types of PSCs are solid nitric acid trihydrate (NAT), supercooled ternary solutions of nitric acid and sulfuric acid in water (STS), and ice or mixtures of these three types [8]. STS clouds are believed to form at the beginning of polar winter when the temperature starts to drop, and nitric acid condenses on sulfate aerosols from the Junge Layer [9,10]. Nitric acid can crystallize at temperatures lower than 195 K and the cloud is then a mixture of STS and NAT [11]. At even lower temperatures (188 K) ice starts to form. Mixtures of PSC types are common, both internal (together in a particle) and external (particles mixed together) are possible [8]. The evidence for this picture is based on extensive laboratory, *in situ* and remote measurements as well as numerical models and simulations [8,10–14]. Measurement methods include aircraft missions [15], balloon borne instrumentation [16], ground based lidar [17] and satellites (for example MIPAS - Michelson Interferometer for Passive Atmospheric Sounding [18–22] and CRISTA - Cryogenic Infrared Spectrometers and Telescopes for the Atmosphere [23]). A new type of PSC is supercooled nitric acid (SNA), composed of a binary mixture of nitric acid and water. Thermodynamic calculations of Carslaw et al. [24] predicted its existence. SNA PSCs were observed by the ILAS-II satellite instrument [25] and most recently by the Atmospheric Chemistry Experiment, ACE [26].

PSCs have been classified for many years based on lidar measurements of the backscatter ratio and depolarization ratio of the returned

* Corresponding author.
E-mail address: llavy@odu.edu (L. Lavy).

https://doi.org/10.1016/j.jqsrt.2023.108827
Received 25 July 2023; Received in revised form 18 October 2023; Accepted 5 November 2023
Available online 7 November 2023

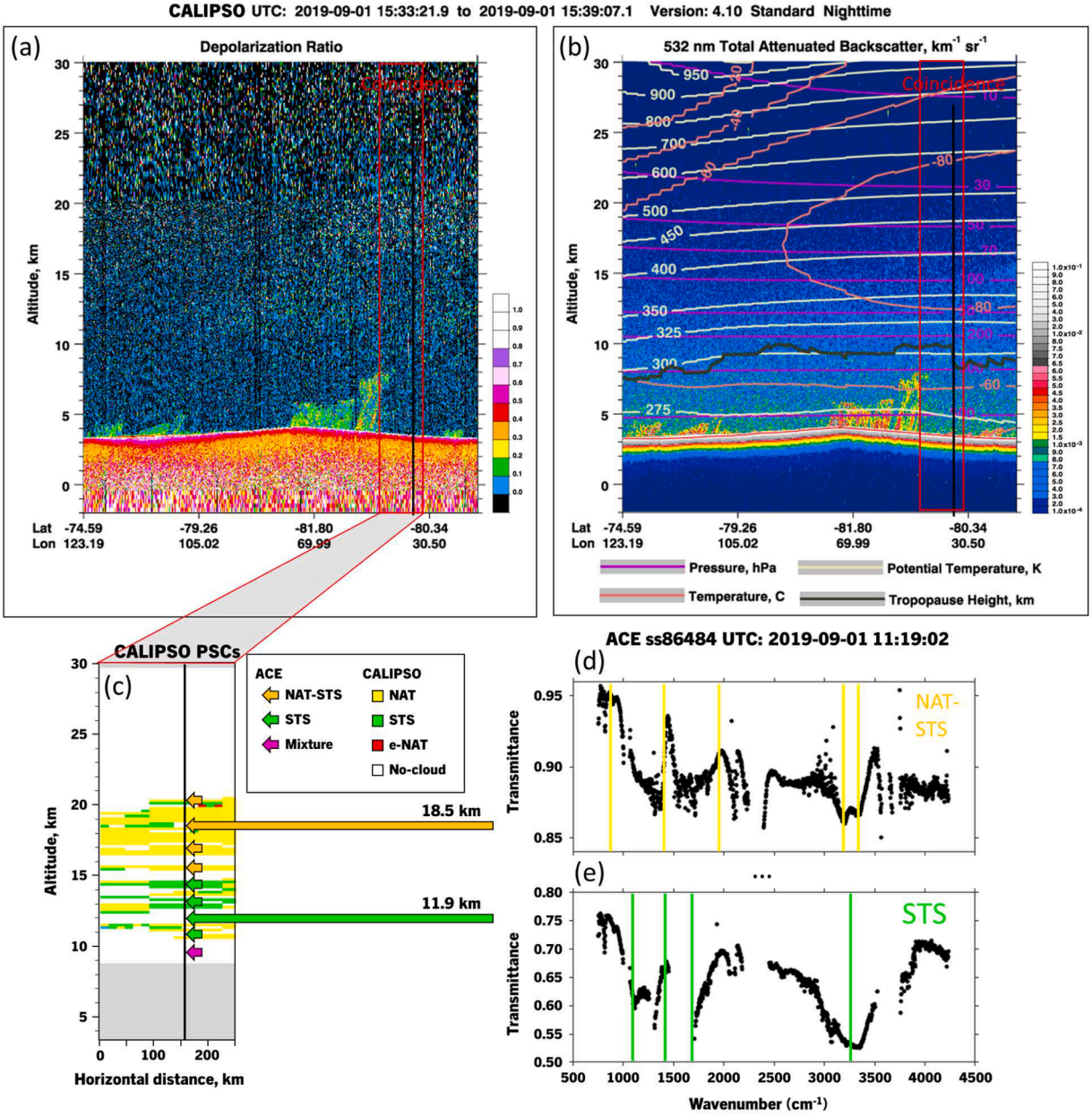

Fig. 1. Example of a coincident observation made by CALIPSO and ACE satellites. (a): Depolarization ratio measured by CALIPSO [43]. The closest point with ACE is shown by a vertical black line and the coincidence zone is shown by a red box. (b): Total attenuated backscatter coefficient at 532 nm. Lines show pressure, potential temperature, temperature, and tropopause height (MET data) (c): CALIPSO determination of PSC composition [30]. The ACE determinations are shown by arrows. (d),(e): ACE residual spectra at 18.5 km and 11.9 km, respectively. The principal features that characterize NAT or STS are shown in color.

signal [27]. Recently, the chemical composition of PSCs by the lidar on the CALIPSO (Cloud-Aerosol Lidar and Infrared Pathfinder Satellite Observations) satellite has been improved [28–30] by using temperature and volume mixing ratios measured with the MLS (Microwave Limb Sounder) on the Aura satellite [31]. The ACE Fourier transform spectrometer has also characterized PSCs with broad band (752–4233 cm^{-1}) infrared transmittance spectra of NAT, STS, SNA and ice [26]. The goal of this article is to compare the composition of PSCs as measured by CALIPSO and ACE for a series of coincident measurements. Profiles and classifications of CALIPSO will be compared with ACE for August 28, 2016, and the 2018 and 2019 Antarctic winters.

2. Methods

The ACE satellite was launched by NASA on August 12, 2003 and has been operational ever since. It orbits at 650 km and at high inclination (74°), giving good coverage of polar regions. The primary instrument aboard the ACE satellite is a high-resolution (0.02 cm^{-1}) Fourier transform spectrometer (FTS) operating within the spectral range of 750–4400 cm^{-1} (2.2–13.3 μm) [32]. The FTS captures sequences of atmospheric transmittance spectra during sunrise and sunset in a limb geometry (solar occultation). These spectra are then processed on the ground [33], enabling the derivation of altitude-dependent concentration profiles [34]. ACE residual spectra are derived by dividing ACE-FTS measurements by a calculated gas-phase spectrum based primarily on the spectroscopic data from the HITRAN2020 database [35] and volume mixing ratio profiles taken from ACE-FTS processing version 5.2 results [36]. The residual spectra are averaged into 2 cm^{-1} wide bins typically providing more than 1000 data points per spectrum. After dividing out all known gas-phase contributions the resulting spectrum is the

spectrum of any underlying cloud or aerosol.

The capabilities of ACE aerosol detection have been reported previously where example spectra were modeled using appropriate optical constants [26,37]. Residual spectra are individually classified by identifying key spectral features that are unique to the aerosol's composition. Identifying the existence or lack of diagnostic features in spectra is a reliable method for accurately classifying aerosol type. The PSC types that ACE is capable of detecting are NAT, STS, ice, SNA and mixtures of these four types. The current classification scheme uses seven categories. First the nearly "pure" PSC spectra (i) NAT, (ii) STS, (iii) ice and (iv) SNA. Pure PSC spectra refer in this paper to spectra overwhelmingly dominated by a single type of PSC. Then three mixed PSC categories: (v) "ice-mix" in which the ice features are clearly distinguishable but other PSC types are present, (vi) NAT-STS mixture where there are no significant ice features, but NAT and STS features are observed and (vii) the "mix" category containing spectra that clearly have aerosols, but it is not clear if they are PSCs. When no cloud is detected, the spectrum is classified as "noise". Note that ACE observations occur exclusively at twilight when the Sun rises or sets through the clouds. The ACE-FTS can measure up to one sunrise and one sunset occultation for each 97 min orbit. Because it is measuring the atmospheric limb, there can be more than one cloud along its line of sight, which is approximately 300 km long with a vertical extent of 2 to 6 km.

The CALIPSO satellite [38] was launched in April 2006 into the A-train satellite constellation, 705 km in altitude, and joined CLOUDSAT in the C-train, 16.5 km below, in September 2018. On board is a lidar called CALIOP (Cloud-Aerosol Lidar with Orthogonal Polarization) that emits a green (532 nm) pulse of polarized light in the nadir direction and detects orthogonally polarized return signals. The latest CALIPSO lidar Level 2 PSC data product [30] was used and it consists of four main classifications: liquid STS, NAT-mixtures, liquid-ice mixtures, and enhanced-NAT mixture (e-NAT). The latter is a sub-class of NAT mixtures representing PSCs with higher number densities of NAT particles. Tropospheric ice clouds are also reported at low altitudes. CALIPSO has also a classification called wave-ice but too few events of this type are coincident with ACE, and therefore it will not be discussed.

PSC classification by CALIPSO is based on coincident CALIOP and MLS observations [28–30]. First, the PSC signal is separated from the aerosol backscatter signal and then the boundaries between the four main classes are computed on a backscatter ratio/depolarization ratio diagram with the help of theoretical calculations [39–41,29]. Additionally, the distinction between NAT mixture or enhanced-NAT mixture and ice is based on theoretical calculations involving temperature, pressure, and HNO_3 and H_2O mixing ratios. The separation between STS and NAT is done with a depolarization threshold and considers the depolarization uncertainty. It is claimed that 10 to 15 % of data points in either class could be misclassified [30]. CALIPSO measures PSC composition with a spatial resolution of 180 m in the vertical direction and 5 km horizontally as a curtain over several thousand kilometers. Observations are limited to nighttime because day light reduces the detection sensitivity. CALIPSO level 1 polar stratospheric cloud composition has been compared to the infrared emission limb sounder Michelson Interferometer for Passive Atmospheric Sounding (MIPAS) during the 2006 Antarctic and 2006/2007 and 2007/2008 Arctic winters [42]. A high correlation of NAT detection between the two instruments was found. More recently, Tritcher et al. [8] compared CALIPSO level 2 PSC composition with MIPAS for spatially homogeneous coincident scenes between 2006 and 2011 and found in addition very good agreement between ice clouds.

In the present study, ACE and CALIPSO measurements are considered coincident when they are less than 150 km apart and occur within a 6 h time window. These criteria were chosen to provide enough coincident events, given the spatial and temporal variability of PSCs. It was observed that the CALIPSO satellite measurement happens systematically at least 1 h after ACE. This is because CALIPSO measures at night while ACE measures at twilight. For high latitude occultations, up to five CALIPSO orbits can meet the criteria for one ACE profile. We chose to compare the ACE vertical profile with the closest CALIPSO profile from all profiles that meet the constraints. CALIPSO's lidar data have high resolution in the vertical direction while the field of view of ACE varies from 2 to 6 km. Therefore, CALIPSO PSC compositions within 4 km of the ACE altitude were used in our analysis. About 23 % of coincidences correspond to a detection of a PSC by ACE and no detection by CALIPSO within the 4 km vertical window. More precisely, about 46 % of the mixture category detected by ACE corresponds to no detection by CALIPSO, 24 % of the NAT-STS detections, 20 % of the ice-mixture detections, 16 % of the STS detections, 15 % of the NAT detections and 11 % of the ice detections. Because we want to focus on the PSC composition detected by both instruments, we restricted our analysis to coincidences with at least one CALIPSO PSC detection within the 4 km vertical window.

3. Results

3.1. Profile comparison

Coincidences were sought for all Antarctic PSC detections made with ACE for three data sets: the day of August 28, 2016, the 2018 winter (from June 1 to October 4) and the 2019 winter (July 11 to September 6). Coincidences were found only late during the season.

Fig. 1 shows an example of a coincident observation made by CALIPSO and ACE. The raw data for the depolarization ratio and total attenuated backscatter coefficients at 532 nm as measured by CALIPSO is shown on panels (a) and (b) respectively (Data version 4.10 presented in [43]). Meteorological data are taken from the Modern-Era Retrospective analysis for Research and Applications, Version 2 (MERRA-2) model [44,45], interpolated to the CALIPSO measurement locations in version 4.10. Note that the lidar data shown is attenuated by aerosol signal and the PSC detection algorithm removes this attenuation. CALIPSO determination of PSC composition in the coincidence zone (in red) is shown and compared to ACE on panel (c). ACE residual infrared transmittance spectra of PSCs at 18.5 km and 11.9 km are shown on panels (d) and (e). Similar figures for other coincidences can be found in the supplementary materials (Figs. S1–S5).

In Fig. 1 (a) and (b), the strong signals between 0 and 10 km correspond to ground and tropospheric clouds. Stratospheric clouds are detected above the tropopause and in a "cold pool" of about 193 K (-80°C). A zone of higher depolarization ratio around 18 km is associated with NAT, STS and some enhance-NAT detections (see Fig. 1 (c)). Note that there is a change in resolution at 20.2 km in the CALIPSO data. These data are smoothed before the PSC detection algorithm, as explained in [39]. Backscatter enhancements are measured between 10 and 15 km and are associated with STS detection. On Fig. 1 (c) is shown the coincident CALIPSO PSC classification and the ACE classification (colored arrows). The CALIPSO and ACE PSC compositions agree. In Fig. 1 (d), the spectrum at 18.5 km has distinct beta-NAT features: a sharp nitrate band due to the ν_2 out-of-plane bending mode [46] at 821 cm^{-1}, a broad feature at 1384 cm^{-1} (nitrate ν_3 antisymmetric N-O stretching mode [46]), and a characteristic OH stretching doublet at 3209 and 3354 cm^{-1}. Normally there is also a weak NAT feature around and 1840 cm^{-1} which is suppressed in this mixture (nearly pure NAT spectra are presented on Fig. S3). This spectrum has also some STS features, a weak SO_2 feature around 900 cm^{-1} and a broad feature forming around 1120 cm^{-1} and is therefore classified as NAT-STS. The spectrum at 11.9 km however is typical of a nearly pure STS detection. It has a sulfate band at 1120 cm^{-1}, characteristic nitric acid bands at 1420 cm^{-1} (part of a doublet) and 1720 cm^{-1}, and a strong broad OH stretching band at 3300 cm^{-1}. It is not shown in the figure, but above 21 km the ACE residual spectra are mostly noise; this altitude agrees with the top of the clouds detected by CALIPSO. Some ice cloud detections can be seen on Figs. S3–S5 in supplementary materials and corroborate the detection of ice by CALIPSO lidar at this altitude (Fig. 1c). Ice clouds

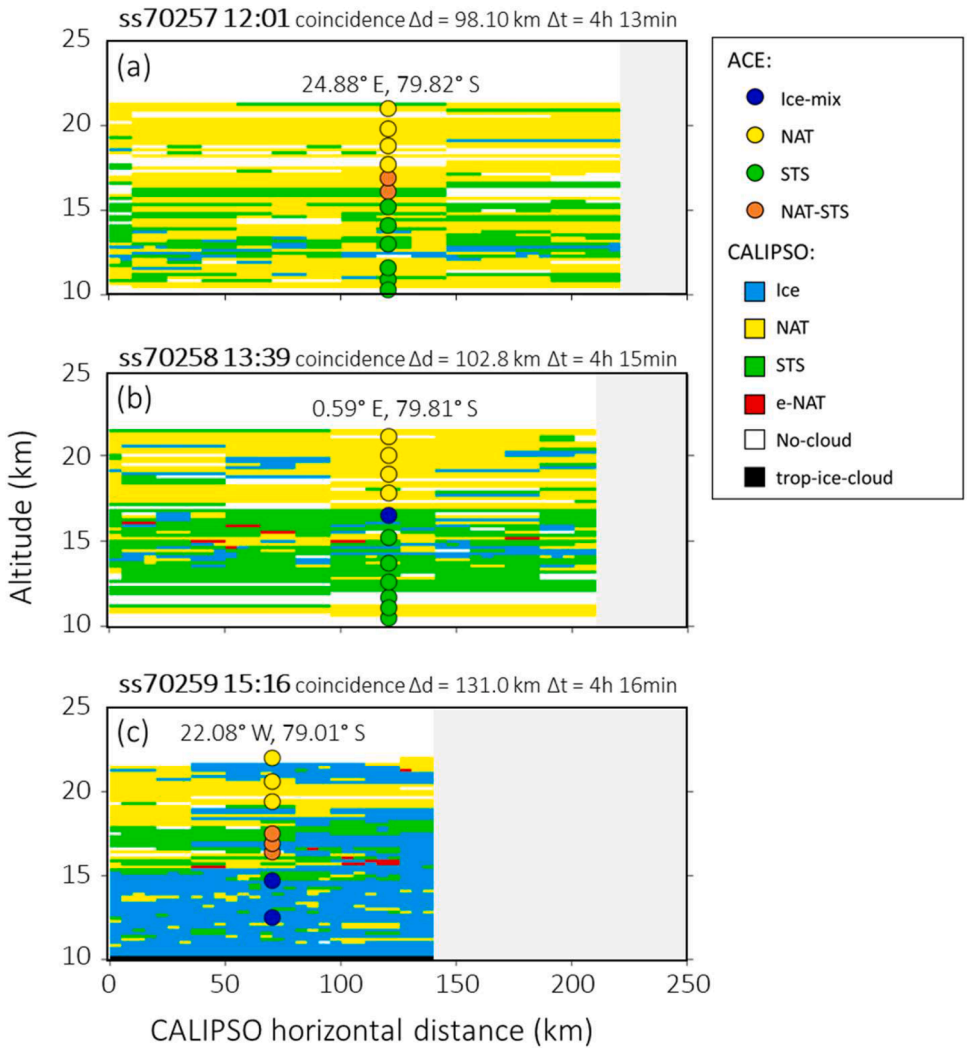

Fig. 2. Comparison of the ACE PSC composition (dots) and the CALIPSO PSC composition (color curtains) for coincidences of three consecutive profiles on August 28, 2016. ACE data points are shown at the position of the closest CALIPSO profile. The origin of the x-axis is the first coincidence in time and all the CALIPSO curtains shown here meet the coincidence constraints (Δd<150 km, Δt<6 h). Each figure includes the ACE sunset identifier (ssXXXXX), UTC time, ACE and CALIPSO profile distance (Δd), CALIPSO's coincidence time relative to ACE (Δt) and ACE profile coordinates. "trop-ice-cloud" stands for tropospheric ice clouds.

have two characteristic upward features at 1000 cm^{-1} and 3550 cm^{-1} [26].

Fig. 2 shows three consecutive sunset measurements made by ACE that coincided with CALIPSO measurements on August 28, 2016. ACE data points are superimposed on the closest CALIPSO horizontal profile. The x-axis origin is fixed to be the first profile in time that meets the coincidence constraints. All the CALIPSO curtains shown meet the coincidence constraints.

For all three coincidences, CALIPSO measured about 4 h after ACE and the measured profiles are 100-130 km apart. In the first coincidence Fig. 2 (a), ACE detects a pure STS cloud below 15 km and a pure NAT cloud above 17 km with a mixture of NAT and STS in the middle. This

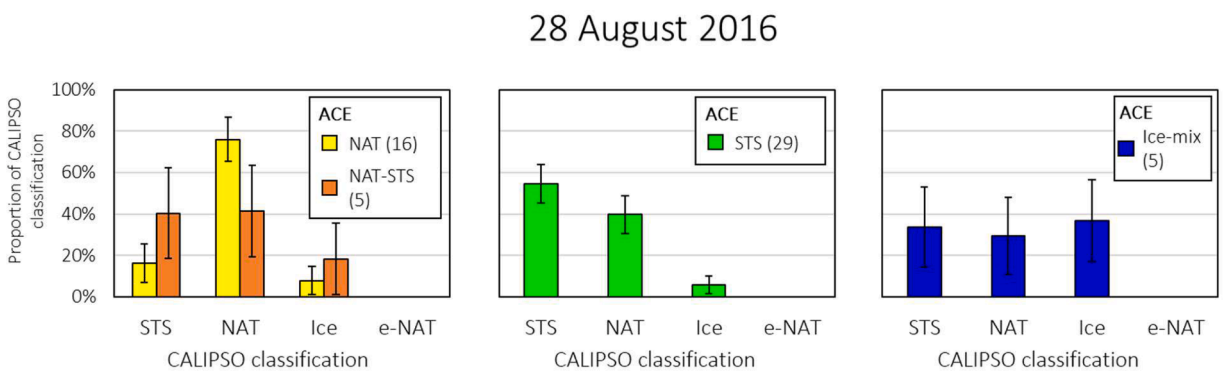

Fig. 3. Comparison of ACE and CALIPSO PSC composition for coincidences during August 28, 2016. For each ACE PSC classification (shown with different colors) the graphs show the proportion of each CALIPSO classification detected in coincidence (x-axis). The number of ACE detections is shown in parenthesis in the legend.

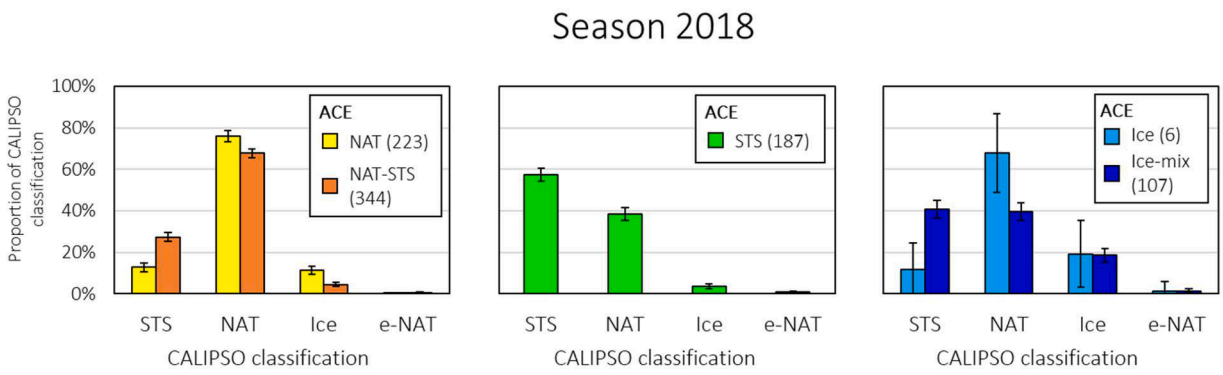

Fig. 4. Comparison of ACE and CALIPSO PSC composition for coincidences during the 2018 winter. See Fig. 3 for detailed description.

agrees with CALIPSO that detects more STS at low altitude and NAT at high altitude. This two-layer cloud with lower altitude STS is typical at the end of the winter [8]. CALIPSO also detects a layer of ice PSCs at low altitude, not detected with ACE. The next coincidence is 1200 km away in Fig. 2 (b). ACE measured 3 layers from top to bottom: NAT, ice mixture and STS. CALIPSO measured mainly NAT and STS but some ice and enhanced-NAT were also present. Fig. 2 (c) shows the third coincidence where mostly ice was detected by CALIPSO. ACE measured ice mixture at low altitude, in agreement with CALIPSO, NAT-STS mixture at 17 km and pure NAT at higher altitudes. CALIPSO also measured a homogenous layer of NAT at high altitude and more STS at middle altitude. The cloud thickness of these coincidences is in agreement. Overall, the CALIPSO data are more heterogenous, with better spatial resolution, while ACE captures a global picture.

3.2. Statistical comparison

For August 28, 2016, 5 coincident profiles were found between the two satellites. This corresponds to 56 ACE PSC detections measured between UTC 10:23 and 20:08 at latitudes from 79.7° S to 80.1° S. In Fig. 3, PSC composition measured by ACE (NAT in yellow, STS in green, ice-mix in dark blue and NAT-STS in orange) is compared with the integrated PSC compositions measured by CALIPSO in the closest profile and within a 4 km vertical window. Error bars represent statistical uncertainty calculated using the number of ACE detections (two times the standard deviation).

For the NAT PSCs (16 detections) detected by ACE (Fig. 3 (a)), the majority of CALIPSO detections within 4 km of ACE's altitude are also NAT (76 %). For STS PSCs (29 detections), a smaller proportion of CALIPSO detections are also STS (54 %), while the other events are NAT (40 %) and ice (6 %). On this day, ACE detected a substantial number of mixtures containing ice (5 detections). They were classified by CALIPSO mainly as ice (37 %) but also as NAT (29 %) and STS (34 %). The NAT-STS mixture detection by ACE was found to correspond in CALIPSO to a similar amount of NAT (41 %) and STS (40 %) and also some ice (18 %). No enhanced-NAT CALIPSO detections were coincident with ACE detections for this day.

A similar analysis was carried for the 2018 and 2019 Antarctic winters. For these winters, coincident profiles were found from August 25, 2018, to September 12, 2018 (180 profiles) and from August 27, 2019 to September 6, 2019 (37 profiles). The coincidence periods are in late winter, despite the larger period probed by ACE. This is because coincidences between the two satellites are more probable when ACE sunsets are observed at higher latitude locations, where CALIPSO scans are more frequent. Coincidence latitudes range from 76.5° S to 82.5° S for 2018 and from 78.3° S to 82.3° S for 2019.

Fig. 4 shows the comparison of ACE and CALIPSO PSC composition for coincidences during the 2018 winter. The same patterns as the single day in 2016 can be observed. Among the NAT PSCs detected by ACE, a large proportion of CALIPSO clouds are also classified as NAT (76 %). STS clouds of ACE are also classified as STS clouds by CALIPSO (57 %). Surprisingly, the pure ice PSCs detected by ACE are mainly classified as NAT (76 %) rather than ice (19 %) by CALIPSO. These numbers must be considered with care considering the low statistics (6 detections), but both NAT and ice are solid particles that could be difficult to tell apart with CALIPSO. Ice-mixture PSCs detected by ACE (107 detections) are classified by CALIPSO as NAT (39 %), STS (41 %) and less frequently as ice (19 %) and enhanced-NAT (1 %). Interestingly, for the mixture classes a lower agreement between ACE and CALIPSO is observed compared to the nearly pure classes. The proportion of agreement goes from 76 % to 68 % for NAT and from 19 % to 18.5 % for ice when changing from ACE's nearly pure PSC detections to mixture PSC detections. Some of the disagreement observed between ACE and CALIPSO is likely due to inhomogeneity within the ACE field-of-view.

Fig. 5 shows the comparison of ACE and CALIPSO PSC composition for coincidences during the 2019 winter. Similar patterns than for the 2018 and 2016 winters are observed. The majority of NAT PSCs are well classified by CALIPSO. For STS clouds, CALIPSO detects large number of

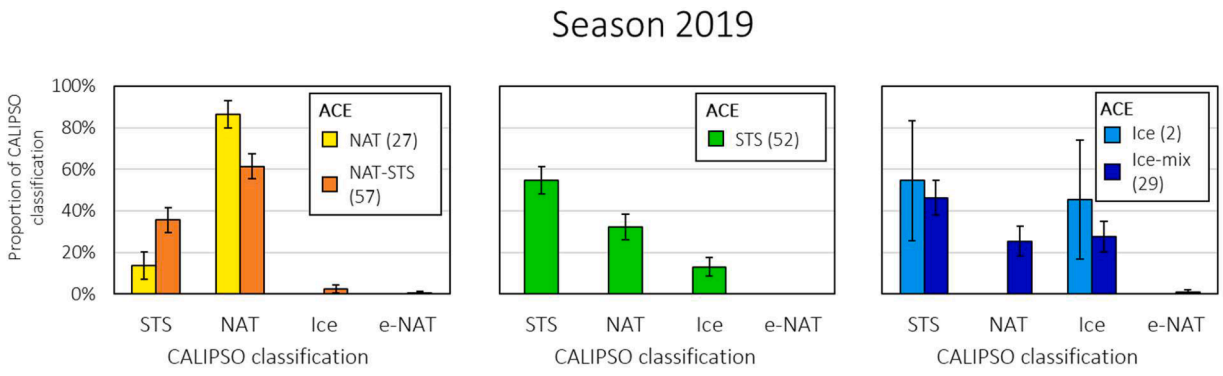

Fig. 5. Comparison of ACE and CALIPSO PSC composition for coincidences during the 2019 winter. See Fig. 3 for detailed description.

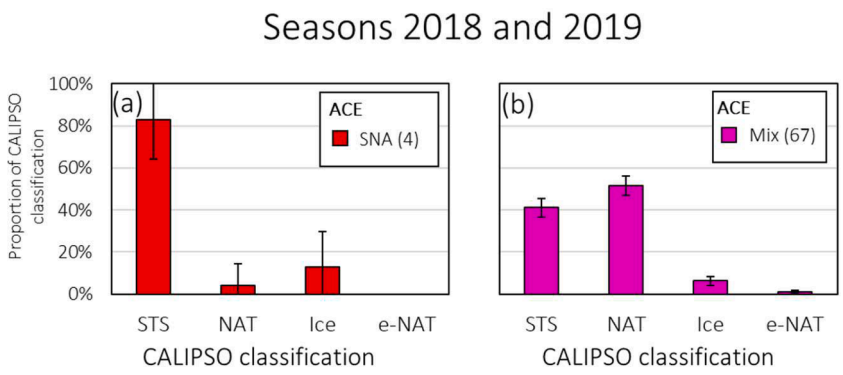

Fig. 6. Comparison of ACE and CALIPSO PSC composition for coincidences during seasons 2018 and 2019 and for the ACE events of SNA PSCs (a) and mixture (b). See Fig. 3 for detailed description.

STS, less NAT and less ice. For ice clouds, CALIPSO detections contain a majority of STS, then ice and NAT.

Enhanced-NAT is relatively uncommon in the CALIPSO data, and its detection is rare. In the 2018 dataset, we found that 60 % of the enhanced-NAT events in coincidence are associated to mix-ice and NAT-STS ACE detections. Ice could be mistaken for NAT by CALIPSO since both of these PSCs contain solid particles with high depolarization ratios.

Some PSCs of the 2018 and 2019 seasons were also recorded as SNA by ACE. In Fig. 6 (a), the red histogram shows the proportion of CALIPSO classifications coincident with SNA detection in ACE. The majority of CALIPSO classifications are STS for this type of cloud (83 %). SNA and STS clouds consist of liquid particles, which are hard to tell apart with lidar alone.

Some ACE's PSC detections are hard to categorize and are therefore labeled as "mixture" PSCs. Fig. 6 (b) shows in pink the comparison for the mixture PSCs with the CALIPSO classification. The mixture PSCs are classified by CALIPSO mainly as NAT (51 %) and STS (41 %).

4. Conclusion

Coincidences between CALIPSO and ACE measurements were found in three time periods which allowed their PSC classifications to be compared. We found general agreement between ACE and CALIPSO even though the measurements are based on completely different optical phenomena. Some disagreements must nevertheless be highlighted. For NAT clouds, the CALIPSO data agrees very well with ACE, with the percentage of misclassification close to the 10-15 % estimated in the classification method. ACE's STS clouds, however, are often coincident with NAT and ice CALIPSO detections. For ACE's ice clouds, approximately one third of the CALIPSO detections are ice, while the rest are NAT and STS. CALIPSO's NAT classification might be too inclusive considering all these results. However, some of the disagreement we found is likely due to inhomogeneity within the ACE field of view. SNA clouds for the 2018 and 2019 winters were detected by CALIPSO as STS. Qualitatively, the proportion of CALIPSO detections is consistent with the different mixture clouds detected in ACE, showing that both CALIPSO and ACE are sensitive to changes in mixture composition. This initial comparison of the ACE PSCs composition classification with CALIPSO shows ACE's potential in characterizing PSCs. ACE has been measuring since February 2004 and its PSC composition analysis has great potential to constrain and to improve current atmospheric models.

CRediT authorship contribution statement

Léo Lavy: Investigation, Formal analysis, Visualization, Writing – original draft, Writing – review & editing. **Peter Bernath:** Investigation, Supervision, Writing – review & editing. **Michael Lecours:** Investigation, Data curation, Writing – review & editing. **Dylan English:** Investigation, Data curation, Writing – review & editing. **Michael Fromm:** Investigation, Visualization, Writing – review & editing.

Declaration of Competing Interest

The authors declare that they have no known competing financial interests or personal relationships that could have appeared to influence the work reported in this paper.

Data availability

Data will be made available on request.

Acknowledgement

The ACE mission is funded by the Canadian Space Agency (9F045-200575/001/SA). Some support was provided by NASA through the Atmospheric Composition Modeling and Analysis Program (80NSSC23K0999). PB acknowledges RB for productive discussion.

Supplementary materials

Supplementary material associated with this article can be found, in the online version, at doi:10.1016/j.jqsrt.2023.108827.

References

[1] Montreal protocol on substances that deplete the ozone layer 1987. https://ozone.unep.org/treaties/montreal-protocol.
[2] Scientific assessment of ozone depletion: 2018. https://csl.noaa.gov/assessments/ozone/2018/.
[3] Molina MJ, Rowland FS. Stratospheric sink for chlorofluoromethanes: chlorine atom-catalysed destruction of ozone. Nature 1974;249(5460):810–2. https://doi.org/10.1038/249810a0.
[4] Solomon S. Stratospheric ozone depletion: a review of concepts and history. Rev Geophys 1999;37(3):275–316. https://doi.org/10.1029/1999RG900008.
[5] Solomon S, Garciat RR, Rowland FS, Wuebbles DJ. On the depletion of Antarctic ozone. Nature 1986;321:755–8. https://doi.org/10.1038/321755a0.
[6] Farman JC, Gardiner BG, Shanklin JD. Large losses of total ozone in Antarctica reveal seasonal ClO_x/NO_x interaction. Nature 1985;315:207–10. https://doi.org/10.1038/315207a0.
[7] Von Der Gathen P, Kivi R, Wohltmann I, Salawitch RJ, Rex M. Climate change favours large seasonal loss of Arctic ozone. Nat Commun 2021;12(1):3886. https://doi.org/10.1038/s41467-021-24089-6.
[8] Tritscher I, Pitts MC, Poole LR, Alexander SP, Cairo F, Chipperfield MP, et al. Polar stratospheric clouds: satellite observations, processes, and role in ozone depletion. Rev Geophys 2021;59(2). https://doi.org/10.1029/2020RG000702.
[9] Junge CE, Chagnon CW, Manson JE. Stratospheric aerosols. J Meteorol 1961;18(1):81–108. https://doi.org/10.1175/1520-0469(1961)018<0081:SA>2.0.CO;2.
[10] Carslaw KS, Peter T, Clegg SL. Modeling the composition of liquid stratospheric aerosols. Rev Geophys 1997;35(2):125–54. https://doi.org/10.1029/97RG00078.
[11] Lowe D, MacKenzie AR. Polar stratospheric cloud microphysics and chemistry. J Atmos Sol-Terr Phys 2008;70(1):13–40. https://doi.org/10.1016/j.jastp.2007.09.011.

[12] Burkholder JB, Sander SP, Abbatt J, Barker JR, Cappa C, Crounse JD, et al. Chemical kinetics and photochemical data for use in atmospheric studies, evaluation No. 19. Pasadena: Jet Propulsion Laboratory; 2019. *JPL Publication* 19-5, http://jpldataeval.jpl.nasa.gov.
[13] Murphy DM, Froyd KD, Schwarz JP, Wilson JC. Observations of the chemical composition of stratospheric aerosol particles. Q J R Meteorol Soc 2014;140(681):1269–78. https://doi.org/10.1002/qj.2213.
[14] Peter T. Microphysics and heterogeneous chemistry of polar stratospheric clouds. Annu Rev Phys Chem 1997;48(1):785–822. https://doi.org/10.1146/annurev.physchem.48.1.785.
[15] Molleker S, Borrmann S, Schlager H, Luo B, Frey W, Klingebiel M, et al. Microphysical properties of synoptic-scale polar stratospheric clouds: *in situ* measurements of unexpectedly large HNO_3-containing particles in the Arctic vortex. Atmos Chem Phys 2014;14(19):10785–801. https://doi.org/10.5194/acp-14-10785-2014.
[16] Voigt C. *In situ* mountain-wave polar stratospheric cloud measurements: implications for nitric acid trihydrate formation. J Geophys Res 2003;108(D5):8331. https://doi.org/10.1029/2001JD001185.
[17] Tencé F, Jumelet J, Bouillon M, Cugnet D, Bekki S, Safieddine S, et al. 14 years of lidar measurements of polar stratospheric clouds at the French Antarctic station Dumont d'Urville. Atmos Chem Phys 2023;23(1):431–51. https://doi.org/10.5194/acp-23-431-2023.
[18] Höpfner M. Study on the impact of polar stratospheric clouds on high resolution mid-IR limb emission spectra. J Quant Spectrosc Radiat Transf 2004;83(1):93–107. https://doi.org/10.1016/S0022-4073(02)00299-6.
[19] Höpfner M, Luo BP, Massoli P, Cairo F, Spang R, Snels M, et al. Spectroscopic evidence for NAT, STS, and ice in MIPAS infrared limb emission measurements of polar stratospheric clouds. Atmos Chem Phys 2006;6(5):1201–19. https://doi.org/10.5194/acp-6-1201-2006.
[20] Spang R, Remedios JJ, Kramer LJ, Poole LR, Fromm MD, Konopka P. Polar stratospheric cloud observations by MIPAS on ENVISAT: detection method, validation and analysis of the northern hemisphere winter 2002/2003. Atmos Chem Phys 2005;5:679–92. https://doi.org/10.5194/acp-5-679-2005.
[21] Spang R, Hoffmann L, Höpfner M, Griessbach S, Müller R, Pitts MC, et al. A multi-wavelength classification method for polar stratospheric cloud typesusing infrared limb spectra. Atmos Meas Tech 2016;9(8):3619–39. https://doi.org/10.5194/amt-9-3619-2016.
[22] Spang R, Hoffmann L, Müller R, Grooß JU, Tritscher I, Höpfner M, et al. A climatology of polar stratospheric cloud composition between 2002 and 2012 based on MIPAS/Envisat observations. Atmos Chem Phys 2018;18(7):5089–113. https://doi.org/10.5194/acp-18-5089-2018.
[23] Spang R, Remedios JJ. Observations of a distinctive infra-red spectral feature in the atmospheric spectra of polar stratospheric clouds measured by the CRISTA instrument. Geophys Res Lett 2003;30(16). https://doi.org/10.1029/2003GL017231.
[24] Carslaw KS, Luo BP, Clegg SL, Th P, Brimblecombe P, Crutzen PJ. Stratospheric aerosol growth and HNO_3 gas phase depletion from coupled HNO_3 and water uptake by liquid particles. Geophys Res Lett 1994;21(23):2479–82. https://doi.org/10.1029/94GL02799.
[25] Kim Y, Choi W, Lee KM, Park JH, Massie ST, Sasano Y, et al. Polar stratospheric clouds observed by the ILAS-II in the Antarctic region: dual compositions and variation of compositions during June to August of 2003. J Geophys Res 2006;111(D13):D13S90. https://doi.org/10.1029/2005JD006445.
[26] Lecours M, Bernath P, Boone C, Crouse J. Infrared transmittance spectra of polar stratospheric clouds. J Quant Spectrosc Radiat Transf 2023;294:108406. https://doi.org/10.1016/j.jqsrt.2022.108406.
[27] Achtert P, Tesche M. Assessing lidar-based classification schemes for polar stratospheric clouds based on 16 years of measurements at Esrange, Sweden. J Geophys Res Atmos 2014;119(3):1386–405. https://doi.org/10.1002/2013JD020355.
[28] Lambert A, Santee ML, Wu DL, Chae JH. A-train CALIOP and MLS observations of early winter Antarctic polar stratospheric clouds and nitric acid in 2008. Atmos Chem Phys 2012;12(6):2899–931. https://doi.org/10.5194/acp-12-2899-2012.
[29] Pitts MC, Poole LR, Lambert A, Thomason LW. An assessment of CALIOP polar stratospheric cloud composition classification. Atmos Chem Phys 2013;13(6):2975–88. https://doi.org/10.5194/acp-13-2975-2013.
[30] Pitts MC, Poole LR, Gonzalez R. Polar stratospheric cloud climatology based on CALIPSO spaceborne lidar measurements from 2006 to 2017. Atmos Chem Phys 2018;18(15):10881–913. https://doi.org/10.5194/acp-18-10881-2018.
[31] Waters JW, Froidevaux L, Harwood RS, Jarnot RF, Pickett HM, Read WG, et al. The Earth observing system microwave limb sounder (EOS MLS) on the aura Satellite. IEEE Trans Geosci Remote Sens 2006;44(5):1075–92. https://doi.org/10.1109/TGRS.2006.873771.
[32] Bernath PF. The Atmospheric Chemistry Experiment (ACE). J Quant Spectrosc Radiat Transf 2017;186:3–16. https://doi.org/10.1016/j.jqsrt.2016.04.006.
[33] Boone CD, Bernath PF, Cok D, Jones SC, Steffen J. Version 4 retrievals for the Atmospheric Chemistry Experiment Fourier transform spectrometer (ACE-FTS) and imagers. J Quant Spectrosc Radiat Transf 2020;247:106939. https://doi.org/10.1016/j.jqsrt.2020.106939.
[34] Bernath PF, Crouse J, Hughes RC, Boone CD. The Atmospheric Chemistry Experiment Fourier transform spectrometer (ACE-FTS) version 4.1 retrievals: trends and seasonal distributions. J Quant Spectrosc Radiat Transf 2021;259:107409. https://doi.org/10.1016/j.jqsrt.2020.107409.
[35] Gordon IE, Rothman LS, Hargreaves RJ, Hashemi R, Karlovets EV, Skinner FM, et al. The HITRAN2020 molecular spectroscopic database. J Quant Spectrosc Radiat Transf 2022;277:107949. https://doi.org/10.1016/j.jqsrt.2021.107949.
[36] Boone CD, Bernath PF, Lecours M. Version 5 Retrievals for ACE-FTS and ACE-Imagers. J Quant Spectrosc Radiat Transf 2023;310:108749. https://doi.org/10.1016/j.jqsrt.2023.108749.
[37] Lecours MJ, Bernath PF, Sorensen JJ, Boone CD, Johnson RM, LaBelle K. Atlas of ACE spectra of clouds and aerosols. J Quant Spectrosc Radiat Transf 2022;292:108361. https://doi.org/10.1016/j.jqsrt.2022.108361.
[38] Winker DM, Vaughan MA, Omar A, Hu Y, Powell KA, Liu Z, et al. Overview of the CALIPSO Mission and CALIOP Data Processing Algorithms. J Atmos Ocean Technol 2009;26(11):2310–23. https://doi.org/10.1175/2009JTECHA1281.1.
[39] Pitts MC, Thomason LW, Poole LR, Winker DM. Characterization of polar stratospheric clouds with spaceborne lidar: CALIPSO and the 2006 Antarctic season. Atmos Chem Phys 2007;7:5207–28. https://doi.org/10.5194/acp-7-5207-2007, 2007.
[40] Pitts MC, Poole LR, Thomason LW. CALIPSO polar stratospheric cloud observations: second-generation detection algorithm and composition discrimination. Atmos Chem Phys 2009;9:7577–89. https://doi.org/10.5194/acp-9-7577-2009. 2009.
[41] Pitts MC, Poole LR, Dörnbrack A, Thomason LW. The 2009–2010 Arctic polar stratospheric cloud season: a CALIPSO perspective. Atmos Chem Phys 2011;11(5):2161–77. https://doi.org/10.5194/acp-11-2161-2011.
[42] Höpfner M, Pitts MC, Poole LR. Comparison between CALIPSO and MIPAS observations of polar stratospheric clouds. J Geophys Res 2009;114:D00H05. https://doi.org/10.1029/2009JD012114.
[43] Kar J, Vaughan MA, Lee KP, Tackett JL, Avery MA, Garnier A, et al. CALIPSO lidar calibration at 532 nm: version 4 nighttime algorithm. Atmos Meas Tech 2018;11(3):1459–79. https://doi.org/10.5194/amt-11-1459-2018.
[44] Molod A, Takacs L, Suarez M, Bacmeister J. Development of the GEOS-5 atmospheric general circulation model: evolution from MERRA to MERRA2. Geosci Model Dev 2015;8(5):1339–56. https://doi.org/10.5194/gmd-8-1339-2015.
[45] Gelaro R, McCarty W, Suárez MJ, Todling R, Molod A, Takacs L, et al. The modern-era retrospective analysis for research and applications, version 2 (MERRA-2). J Clim 2017;30(14):5419–54. https://doi.org/10.1175/JCLI-D-16-0758.1.
[46] Nakamoto K. Infrared and Raman spectra of inorganic and coordination compounds. 5th ed. New York: Wiley; 1997. Part A.